1 Main Ionizing Radiation Types and Their Interaction with Matter

Boris I. Kharisov
Universidad Autónoma de Nuevo León

Oxana V. Kharissova
Universidad Autónoma de Nuevo León

CONTENTS

1.1 INTRODUCTION

A grand variety of old and modern techniques is used nowadays for processing materials and composites, including classic methods of wet chemistry, high-temperature sinterization, arc discharge and other electrochemical processes, microwaves and ultrasound, chemical vapor deposition, and flame synthesis among many others (Hinklin and Lu, 2009; Yi et al., 2010). During the last 20 years,

a considerable attention has been paid to the fabrication of nanomaterials and nanocomposites (Schodek et al., 2009). At the same time, among the techniques based on various types of irradiation, only laser ablation and UV radiation are relatively common methods in comparison with the application of classic ionizing radiation. However, the ionizing radiation is also a high-efficiency tool, which can be successfully applied for obtaining novel materials and for the modification of those already known. Various aspects of the interaction of ionizing radiation with matter have been recently discussed in a series of books and chapters (Lilley, 2001; L'Annunziata, 2003; Mozumder and Hatano, 2003; Leroy and Rancoita, 2009; Kharisov et al., 2012; Nikjoo et al., 2012), reviews (Ehlermann, 2002; Bertoni, 2003; Turner, 2004, 2005; Drobny, 2005; Koprda, 2005; Inokuti, 2006; Park, 2006; Chmielewski, 2007; Banhart, 2008; Trapp and Johnston, 2008; Savchenko and Dmitriev, 2010; Shpak and Molodkin, 2010), and educational sites (Larson, 2012; Nave, 2012; Piccard, 2012; Sprawls, 2012).

In this introductory chapter, we present the types and main properties of the ionizing radiation and general description of its interaction with matter. In addition, taking into account that some other chapters of the present book are dedicated, in particular, to the synthesis of materials using β-particles and γ-irradiation, here in the present chapter we will carry out the analysis of examples of more rare application of α-particles, x-rays, neutrons, protons, and ion beams for obtaining various materials, composites, and chemical compounds.

1.2 BRIEF CLASSIC DESCRIPTION OF IONIZING RADIATION

1.2.1 Types of Ionizing Radiation

According to the classic definition, *ionizing radiation* (Figure 1.1) is a flux of subatomic particles (e.g., photons, electrons, positrons, protons, and nuclei) that cause ionization of atoms of the medium through which the particles pass. The radiation is isotropic: leaving the atom, it cannot go

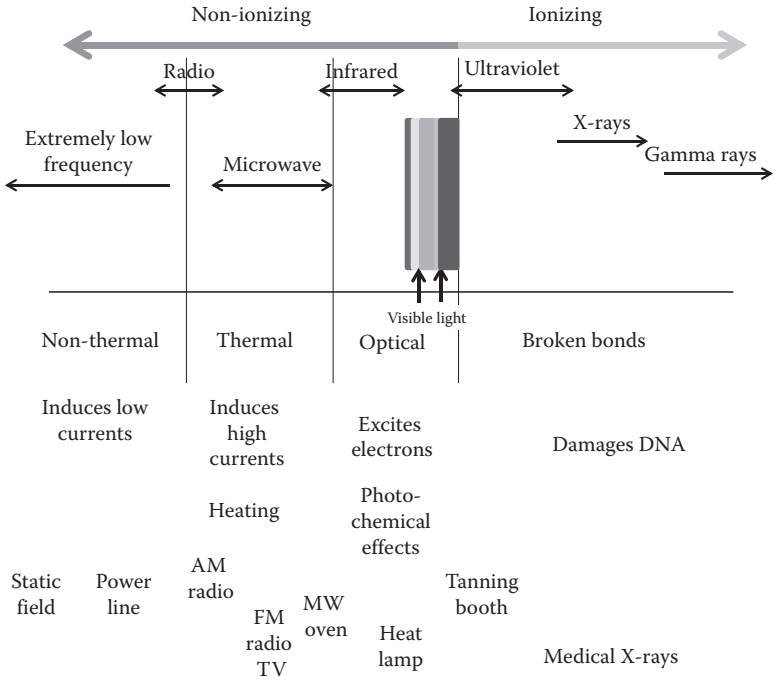

FIGURE 1.1 Ionizing and nonionizing radiations. (From http://www.epa.gov/rpdweb00/understand/ionize-nonionize.html)

TABLE 1.1
Main Radiation Types and Their Sources

Irradiation Type/Description	Sources/Equipment Used for the Synthesis of Composites
Ionizing Radiation	
Alpha (α, helium nuclei), 4–9 MeV	α-emitting isotopes and accelerators of elemental particles
β^-/e^- beam (β^- particles or accelerated electrons), velocity less than the velocity of light, energy 10 keV–10 MeV (positrons β^+ belong to the same range)	Electronic accelerator
Gamma (γ)-rays (velocity 3×10^8 m/s in free space), wavelength < 0.1 nm, energy > 10 keV	^{60}Co
X-rays, wavelength 10–0.001 nm, energy 100 eV–1 MeV	Synchrotron radiation source
Neutrons (*n*)	Nuclear reactor and laboratory sources: ^{252}Cf, ^{241}Am/Be {(α;n) reaction on the beryllium: ^{9}Be(α;n)^{12}C}.
Thermal neutrons <0.4 eV	
Intermediate neutrons 0.4 eV–200 keV	Neutron generators (neutron source devices that contain compact linear accelerators and that produce neutrons by fusing isotopes of hydrogen together): $D + D \rightarrow {}^3\text{He} + n$ (2.5 MeV) $D + T \rightarrow {}^4\text{He} + n$ (14.1 MeV)
Fast neutrons >200 keV	
Protons (*p*)	Cyclotron
Ion beam {swift heavy ions: positively charged ions of a series of metals (Ni, Ag, Li, Ge, Co), C, Si, O, inert gases, etc.}	Cyclotron resonance ion source
Nuclear fragments and recoil nuclei, energy 1–100 MeV	
Ultraviolet (UV) light (whole range 400–15 cm^{-1}): UV radiation with wavelengths *shorter than 124 nm* (mid-vacuum UV) is ionizing radiation	High-power UV lamps

in one direction. *Ionization* means the removal of electrons from atoms of the medium. In order to remove an electron from an atom, a certain amount of energy must be transferred to the atom. According to the law of conservation of energy, this amount of energy is equal to the decrease in kinetic energy of the particle that causes ionization. Therefore, ionization becomes possible only when the energy of incident particles (or of the secondary particles that may appear as a result of interactions of incident particles with matter) exceeds a certain threshold value—the *ionization energy* of the atom. The ionization energy for gas molecules is usually of the order of 34 eV ($1\ \text{eV} = 1.6022 \times 10^{-19}$ J).

Ionizing radiation (Table 1.1) may be of distinct nature. The *directly ionizing radiation* is composed of high-energy charged particles, which ionize atoms of the material due to Coulomb interaction with their electrons. Such particles are, e.g., high-energy electrons and positrons (β-radiation), high-energy ^{4}He nuclei (α-radiation), and various other nuclei, e.g., accelerated metal ions (ion beams). *Indirectly ionizing radiation* is composed of neutral particles that do not directly ionize atoms or do that very infrequently, but due to interactions of those particles with matter, high-energy free charged particles are occasionally emitted. The latter particles directly ionize atoms of the medium. Examples of indirectly ionizing radiation are high-energy photons (ultraviolet, x-ray, and gamma radiation) and neutrons of any energy (neutrons are special and interact only with nuclei).

Main types of radioactive decay are as follows: (1) α-*decay* (e.g., $^{226}_{88}\text{Ra} \rightarrow {}^{222}_{86}\text{Rn} + \alpha$), which is typical for radioactive elements with high atomic number Z; (2) β-*decay* (e.g., $^{140}_{56}\text{Ba} \rightarrow {}^{140}_{57}\text{La} + \beta^-$), which is typical for many radioactive isotopes having relative excess of neutrons in the nucleus;

(3) β^+-*decay* (e.g., $^{13}_{7}N \rightarrow {}^{12}_{6}C + \beta^+$), which is observed mostly in case of artificial radioactive isotopes having excess of protons; (4) *K-capture* (e.g., $^{64}_{29}Cu \rightarrow {}^{64}_{28}Ni$), which is also observed mostly in case of artificial radioactive isotopes having excess of protons (this type of decay depends very slightly on the chemical state of the transforming atoms; characteristic x-ray irradiation or Auger electrons could also accompany this process); (5) *isomer transition* (e.g., $^{80*}_{35}Br \rightarrow {}^{80}_{35}Br + \gamma$) (strictly, this is not a type of radioactive decay); (6) *emission of proton or neutron* (strictly, this is not a type of radioactive decay), *or spontaneous fission*. Emission of neutron can take place in the decay chain, when the energy of excitation of daughter nucleus exceeds the bond energy of the neutron (reaction 1.1). Spontaneous fission is the classic case for uranium, whose nucleus can be divided into two light nuclei, e.g., $_{56}Ba$–$_{36}Kr$, $_{54}Xe$–$_{38}Sr$, and two to three neutrons. In addition to these neutrons (prompt neutron is a neutron immediately emitted by a nuclear fission event), a *delayed neutron* decay can occur within the same context, emitted by one of the fission products anytime from a few milliseconds to a few minutes later. Similarly, after β^+-decay, a *delayed proton* can be emitted.

$$^{137}_{53}I(-\beta^-) \rightarrow {}^{137}_{54}Xe(-n) \rightarrow {}^{136}_{54}Xe \tag{1.1}$$

γ-*Irradiation* is a special type of decay only by isomer transition. Very frequently, other types of decay are accompanied by γ-irradiation. γ-Rays, emitted by excited nucleus, could interact with orbital electron and eliminate it from the atom. This process is known as *internal conversion* of γ-irradiation. This process can be easily discovered, since the conversion electrons (e^-) possess lineal spectrum, which is different from the continuous spectrum of β^-particles. The internal conversion is always accompanied by characteristic x-ray irradiation, appearing as a result of the secondary filling of the electronic shell.

In addition, Goldanskii in 1960 predicted ground-state *two-proton (2p) emission* (Goldanskii, 1960). Modern theories predicted ^{45}Fe, ^{48}Ni, and ^{54}Zn to be the best candidates (Brown, 1991; Cole, 1996; Ormand, 1996). Also it is necessary to mention *cluster decay* (also named heavy-particle radioactivity or heavy-ion radioactivity), which is a type of nuclear decay in which a parent atomic nucleus with A nucleons and Z protons emits a cluster of N_e neutrons and Z_e protons heavier than an alpha particle but lighter than a typical binary fission fragment (although ternary fission into three fragments produces products that overlap cluster decay). A chemical transformation of the parent nucleus leads to a different element, the daughter, with a mass number $A_d = A - A_e$ and atomic number $Z_d = Z - Z_e$, where $A_e = N_e + Z_e$. For example, $^{223}_{88}Ra \rightarrow {}^{14}_{6}C + {}^{209}_{82}Pb$ (Poenaru and Greiner, 2011). This type of rare decay mode was observed in radioisotopes that decay predominantly by alpha emission, and it occurs only in a small percentage of decays for all such isotopes. The cluster decay is one of the most important discoveries of the twentieth century.

The mechanism of interaction of particles with matter depends on the nature of the particles (especially on their mass and electric charge). Depending on the manner in which particles interact with matter, four distinct groups of particles can be defined:

1. Heavy charged particles (such as α-particles and nuclei)
2. Light charged particles (such as electrons and positrons)
3. Photons (neutral particles with zero rest mass)
4. Neutrons (neutral heavy particles)

1.3 INTERACTION OF IONIZING RADIATION WITH MATTER

1.3.1 Nuclear Reactions upon Passing Irradiation through the Matter

Nuclear reactions (which are not the same as radioactive decay), according to current ideas, take place in two steps: (1) fusion of the bombarding particle with the nucleus ($\sim 10^{-21}$ s) and formation

of a compound-nucleus; and (2) decay of the excited compound-nucleus forming reaction products (Lukiyanov et al., 1985). The compound-nucleus exists, before its decay, $\sim 10^{-12}$ s. The decomposition of the compound-nucleus rarely takes place in a single reaction course; in general, several reaction paths are possible. For example, the interaction of $^{27}_{13}$Al with neutrons under bombardment leads, through formation of the $^{28}_{13}$Al compound-nucleus, to five types of reactions: (n,2n), (n,n), (n,γ), (n,p), and (n,α).

It is well known that nuclear reactions are divided into several types depending on the type of bombarding particles. The following reactions are possible: by action of neutrons n, protons p, deuterons d, tritons t, α-particles and more heavy nuclei, as well as γ-rays. The energy of bombarding particles has a considerable role. If the reaction takes place using charged particles (or charged particles or neutrons are formed as a result of reaction), the bombarding particle must have a definite minimum energy to overcome the potential barrier (threshold of the reaction). Such reactions are called threshold reactions. Those reactions that take place at any (even very low) energies of bombarding particles are nonthreshold (for instance, the reaction (n,γ)).

The type and energy of bombarding particles determine directions of nuclear reactions. The reactions (n,n), (p,p), (α,α) are particular cases of inelastic dispersion of the bombarding particle. As a result of such reactions, only nuclear isomers can be formed. If the bombarding and emitted particles have the same charge, the isotopes of the irradiated element are formed. This is resulted by the reactions (n,γ), (n,2n), (d,p), (t,p), (γ,n). The majority of nuclear reactions lead to the formation of nuclei, different from the initial nuclei by their atomic number. The nuclear mass can be conserved, as, e.g., in the reactions (n,p), (p,n), (d,2n), or be changed, decreasing or increasing, for instance, for the reactions (n,α), (n,np), (n,f), (p,α), (p,γ), (d,n), (t,n), (α,n), (α,p) (Zaborenko et al., 1964).

In order to obtain flows of charged particles of a definite energy, the accelerators (for instance, cyclotron) are used. The irradiation with neutrons is carried out in reactors, where powerful flows of neutrons are formed due to the reaction (n,f). At laboratory scale, small sources of neutrons are used, e.g., Ra–Be (reaction ^{9}Be(α,n)^{12}C, $\sim 10^{7}$ neutrons/s, but under a considerable γ-"background") or Po–Be (not only less danger of γ-radiation, but also less neutron yield and low half-life of ^{210}Po [140 days]). Neutron energies for these sources are in the range of 1–8 MeV. To get thermal neutrons, these sources are put inside a moderator, for instance, water or paraffin hydrocarbon.

1.3.2 Interaction of Charged Particles with Matter

1.3.2.1 Interaction of α-Particles with Matter

The penetrative capacity of the irradiation is determined by the character of interaction irradiation with matter; this is important both for selection of its registration technique and for solution of problems of radiation safety. When the irradiation passes through the matter, its energy is spent mainly for ionization and excitation of atoms and molecules of the substance. α-Particles possess low penetrative capacity and strong ionizing action. Their penetration is described by the magnitude of *path*: the length of trajectory in a given substance. The routes of α-particles are usually direct. The distribution of α-particles in the thickness of the layer of absorbing gas is shown in Figure 1.2. Due to the nonhomogeneity of absorbing substance, not all α-particles, having equal initial energy, result in equal path. So, more exact determination of path magnitude is carried out by differentiation of curve 1, showing the distribution of the number of α-particles in the route length. The abscissa of the maximum of the differentiation curve 2 gives the magnitude of medium path of α-particles in substance.

1.3.2.2 Interaction of β-Particles with Matter

In the case of β-particles, their ionizing action in a unit of route length (specific ionization) is less, and their penetrative capacity is accordingly more in comparison with α-particles. Passing through the matter, the β-particles easily disperse. As a result, the trajectories of β-particles in substances exceed 1.5–4 times the thickness of the passed layer. So, the path of β-particles in a substance

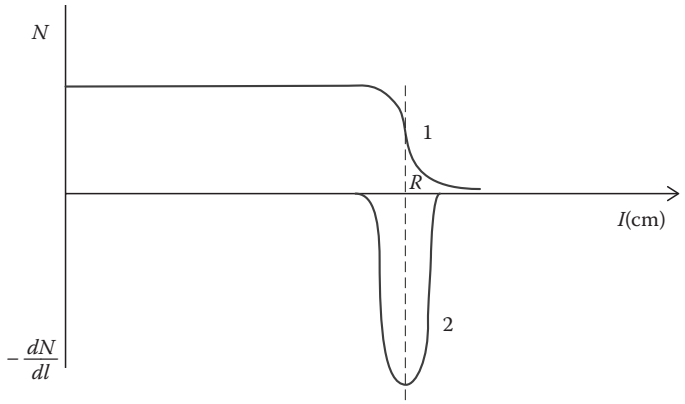

FIGURE 1.2 Dependence of the number of α-particles on the distance from the source. *N* is the number of α-particles on the distance *l*; *−dN/dl* is the number of α-particles with the path *l*; *R* is the medium path of α-particles.

corresponds to the minimal thickness of the absorbent, when almost all electrons of the initial fluent are retained. Since the β-irradiation has continuous energetic spectrum, the penetrative capacity of β-particles is characterized by the magnitude of their maximum path R_{max}. This magnitude corresponds to the path of β-particles with maximum energy in a substance.

The summary process of absorption and dispersion of β-particles is called weakening. The curve of dependence of the number of particles (*N*), passing through the absorbent with a given thickness, on the thickness of weakening layer *d* is shown in Figure 1.3. In order to determine the magnitude of maximum energy of β-spectrum, it is possible to measure the layer of half-weakening of β-irradiation ($d_{1/2}$). This magnitude corresponds to the thickness of the absorbent, decreasing the initial number of particles to one half. For rough evaluation of $d_{1/2}$, the formula $R_{max} = 7.2d_{1/2}$ can be used.

When an electron flow arrives at the surface of a material, a part of particles can be reflected on the angle major 90°. This effect is named as *reverse dispersion of electrons* and used to resolve a series of applied problems, e.g., to determine the width of films. The same effect could be a source of methodical errors, in particular working with electron flows, leading to an increase in the number of particles, and moving to the counter due to their dissipation in the material.

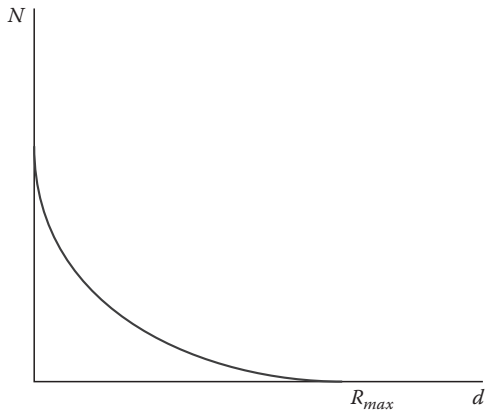

FIGURE 1.3 Curve of attenuation of β-irradiation.

1.3.2.3 Interactions of Protons with Matter

Within the energy range of importance in proton therapy (from stopping protons to ≈250 MeV), it is convenient to consider two energy intervals separately (Sjirk Niels Boon, 1998):

1. Low energy: below ≈0.5 MeV, protons can pick up orbital electrons and form hydrogen. Also energy can be lost to atomic nuclei due to electromagnetic interactions (nuclear stopping power). These are complicated processes, but fortunately they play a role only at the very last micrometers of a proton track. It is important for the subject of *microdosimetry*, which deals with the energy loss process on a microscopic scale (e.g., the study of the effect of ionizing radiation on DNA) (Gottschalk, 2011).
2. High energy: for proton energies between ≈0.5 and 250 MeV, the atoms in the stopping medium can be excited or ionized. The collision process is well understood, and in principle the stopping power can be calculated theoretically.

1.3.2.4 Cherenkov Radiation

There is another mechanism by which *charged particles* can produce electromagnetic radiation. When the particle moves faster than the speed of light in the material, it generates a shock wave of electromagnetic radiation similar to the bow wave produced by a boat traveling faster than the speed of water waves. Cherenkov radiation (Figure 1.4) does not occur at all if the particle's speed is less than the speed of light in the material. Even at high energies, the energy lost by Cherenkov radiation is much less than that by the other two mechanisms, but it is used in radiation detectors where the ionization along the track cannot be conveniently measured, e.g., in large volumes of transparent materials. Flashes of Cherenkov light are produced when cosmic rays enter the Earth's atmosphere.

1.3.2.5 Bremsstrahlung

Bremsstrahlung is an electromagnetic radiation produced by the deceleration of a charged particle when deflected by another charged particle, typically an electron by an atomic nucleus. The moving particle loses kinetic energy, which is converted into a photon because energy is conserved. The term is also used to refer to the process of producing the radiation. Bremsstrahlung has a continuous spectrum, which becomes more intense and shifts toward higher frequencies when the energy of

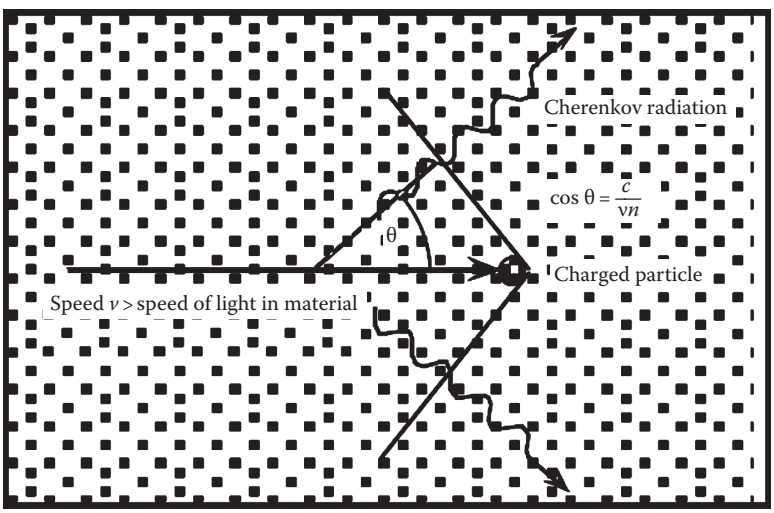

FIGURE 1.4 The speed v of the charged particle is greater than the speed c/n of light in the material; n is the refractive index.

the accelerated particles is increased. Strictly speaking, bremsstrahlung refers to any radiation due to the acceleration of a charged particle, which includes synchrotron radiation and cyclotron radiation; however, it is frequently used in the more narrow sense of radiation from electrons stopping in matter.

1.3.2.6 Overview of the Electromagnetic Interactions of Charged Particles

The electromagnetic interactions of charged particles with a kinetic energy in the range 100 keV to a few 10 MeV are summarized in the following (Tavernier, 2010).*

Electrons: Electrons lose energy by exciting and ionizing atoms along their trajectory. Per centimeter, electrons will lose about 2 MeV multiplied by the density. Electrons typically travel several centimeters before losing all their energy. The trajectories of electrons are erratically twisted due to multiple scattering. They will also lose a significant fraction of their energy by bremsstrahlung, particularly at higher energies. If the energy exceeds 264 keV, electrons show Cherenkov radiation in water.

Positrons: Positrons behave in exactly the same way as electrons except that, after coming to rest, a positron will annihilate with electrons that are always present. This annihilation gives rise to a pair of back-to-back gamma rays of 511 keV.

Alpha particles: The energy loss of alpha particles is much larger than that of electrons. It is of the order of 1000 MeV/cm times the density of the medium. As a result, alpha particles travel only tens of micrometers in solids and a few centimeters in gases. The trajectory of alpha particles is approximately straight.

Protons: Protons ionize much more than electrons but less than alpha particles. The range in solids is of the order of 1 mm. The trajectory of protons is approximately straight.
Nuclear fragments: Nuclear fragments show extremely high ionization, and therefore the range of such nuclear fragments is typically only a few micrometers long.

1.3.3 Interaction of Gamma Radiation with Matter

As in the case of charged particles (e.g., electrons, protons, α-particles), interaction of photons of γ-radiation with matter is of electromagnetic nature. However, the exact physical mechanism of that interaction is quite different than that in the case of charged particles because of the following:

1. Photons do not have electric charge; therefore, they do not participate in Coulomb interaction. Photon interaction cross section is much smaller than interaction cross sections of charged particles.
2. The photon rest mass is zero; therefore, their velocity is always equal to the velocity of light. That is, photons can*not* be slowed down in matter (unlike charged particles). Photons can be only scattered or absorbed.

Photon *absorption* is an interaction process when the photon disappears, and all its energy is transferred to atoms of the material or to secondary particles. Photon *scattering* is an interaction process when the photon does not disappear, but changes the direction of its propagation. In addition, the scattered photon may transfer a part of its energy to an atom or an electron of the material. There are two interaction processes whereby a photon is absorbed and several types of scattering (of which one type is much more important than the others).

Photoelectric effect (Figure 1.5) is a type of interaction of a photon with an atom when the atom absorbs all energy of the photon (i.e., the photon disappears) and one of atomic electrons (called

* The same reference describes the interactions of neutrino with matter (p. 49).

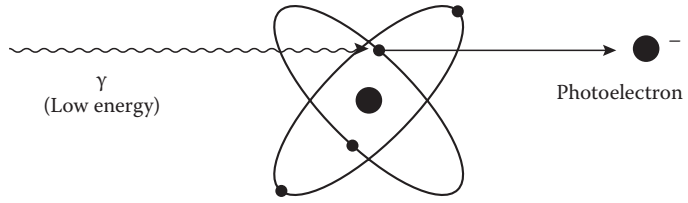

FIGURE 1.5 Photoelectric effect.

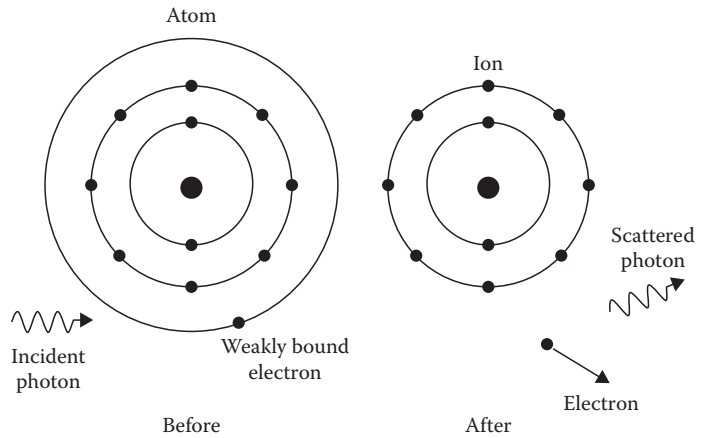

FIGURE 1.6 Compton scattering by a weakly bound electron.

photoelectron) is removed from the atom. The atomic cross section of the photoelectric effect is characterized by an especially strong dependence on the atomic number Z of the material and on photon energy. When photon energy is of the order of 100 keV, the just-mentioned cross section is approximately equal to $\sigma_f \approx 10^{-37} Z^5/(h\nu)^{7/2}$, where the cross section σ_f is expressed in square meter and $h\nu$ is the photon energy in megaelectron volt. It follows that photoelectric effect cross section rapidly increases with increasing atomic number Z and decreasing photon energy $h\nu$.

Compton scattering (Figure 1.6). From the quantum mechanical point of view, a scattering event is a collision of two particles—a photon and an electron or a photon and an atom. From the laws of conservation of energy and momentum, it follows that due to scattering by electrons of the material, photon energy must decrease (because a part of that energy must be transferred to the electrons). This effect, which was first described in 1922 by American physicist A. Compton, became one of the cornerstones of quantum mechanics, because it proved that electromagnetic radiation under certain circumstances behaves like particles. Such type of scattering, when photon energy decreases, is called *Compton scattering*. When photon energy is large (of the order of 10 keV or more), Compton scattering is the dominant scattering mechanism. Since a single Compton scattering event is a result of photon's interaction with a single electron, the *atomic* Compton scattering cross section σC is equal to the *electronic* Compton scattering cross section σ times the number of electrons in an atom (the latter number is equal to the atomic number Z): $\sigma C = Z\sigma$. By definition, σ does not depend on Z. Thus, the atomic Compton scattering cross section is directly proportional to the atomic number of the material. When the photon energy is sufficiently large (of the order of 100 keV or larger), σ decreases with increasing photon energy.

Electron–positron pair production (Figure 1.7). In the electric field of an atomic nucleus, a photon may stop existing by transforming all its energy into relativistic energy of two new particles—a free electron and a positron (electron's antiparticle). Since the recoil energy of the nucleus is relatively small, the law of conservation of energy during such an event can be written as follows:

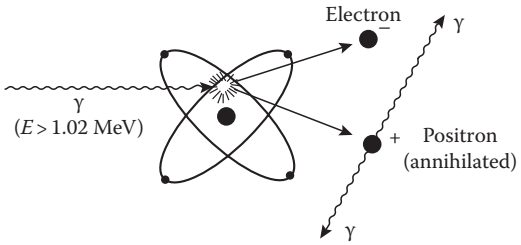

FIGURE 1.7 Electron–positron pair production.

$h\nu = m_+c^2 + m_-c^2$, where m_+c^2 and m_-c^2 are the total relativistic energies of the positron and the electron, respectively (m_+ and m_- are the total relativistic masses of the positron and the electron). Since m_+ and m_- are always larger than the electron's rest mass m_0, it follows that pair production is possible only when photon energy is larger than two rest energies of an electron: $2m_0c^2 \approx 1.02$ MeV. This is the so-called threshold energy of pair production. Although pair production becomes possible when photon energy exceeds the mentioned threshold value, the pair production cross section σp exceeds the Compton scattering cross section σC only when the photon energy approaches and exceeds 10 MeV. At smaller photon energies, the frequency of pair production events is much smaller than the frequency of Compton scattering events.

It is necessary to mention that the positron, entering into the solid matter, forms a pair with the electron (positronium Ps), which itself (Ps) migrates to the solid phase (about 10^{-6}–10^{-5} s). Meeting with defects of crystal structure, the electron and positron annihilate. This method can be used for the determination of defect and size distribution in solids. The diffusion coefficient of Ps is 0.1 cm^2/s.

Electron–photon cascades (Figure 1.8). *Bremsstrahlung* by a high-energy electron results in a high-energy photon as well as a high-energy electron. Pair production by high-energy photons results in a high-energy electron and a high-energy positron. In both cases, two high-energy particles are produced from a single incident particle. Furthermore, the products of one of these processes can be the incident particles for the other. The result can be a cascade of particles that increases in number while decreasing in energy per particle, until the average kinetic energy of the electrons falls below the critical energy. The cascade is then absorbed by ionization losses. Such cascades, or showers, can penetrate large depths of material.

The attenuation coefficient. The total cross section of interaction of a gamma radiation photon with an atom is equal to the sum of all three mentioned partial cross sections: $\sigma = \sigma_C + \sigma_f + \sigma_p$. Depending on the photon energy and the absorber material, one of the three partial cross sections

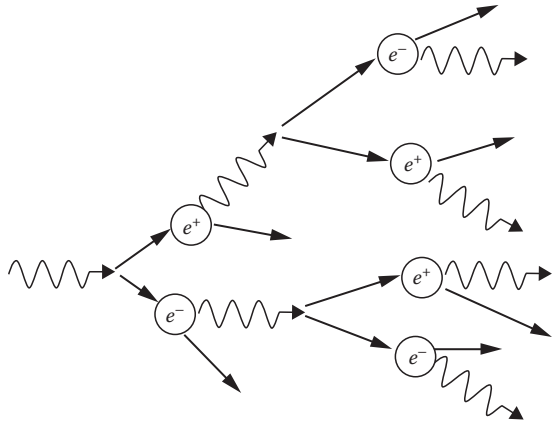

FIGURE 1.8 An electron–photon cascade.

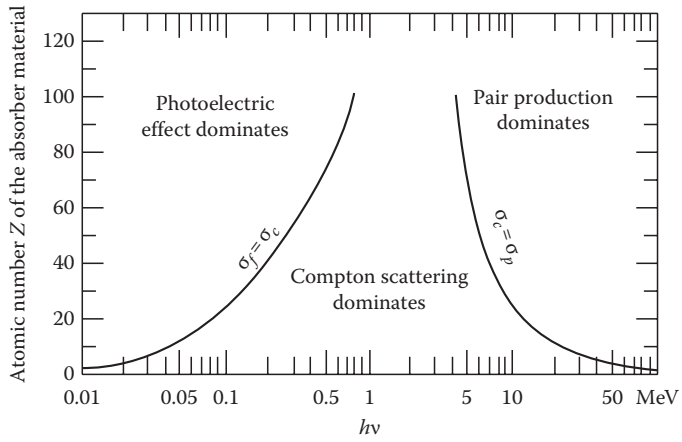

FIGURE 1.9 The relative importance of various processes of γ-radiation interaction with matter.

may become much larger than the other two. Then the corresponding interaction process is the dominant one. Figure 1.9 shows the intervals of photon energy $h\nu$ and atomic number Z corresponding to the case when one of the three interaction processes dominates. Obviously, the photoelectric effect dominates at small values of photon energy (1–100 keV), Compton scattering dominates at intermediate energies (100 keV–1 MeV), and pair production dominates at high energies (above 1 MeV). The width of the energy interval corresponding to the Compton effect increases with decreasing atomic number of the material.

1.3.4 Interaction of Neutrons with Matter

Neutrons, being uncharged, do not interact electromagnetically with electrons or nuclei in matter. Instead, the nuclear interaction with nuclei is the most common interaction, but this can occur only if the neutron comes within 1 fm of the nucleus. Hence, the attenuation coefficient for neutrons is small and neutrons can penetrate large amounts of matter. The main interaction processes are elastic scattering $\{A(n,n)A\}$, inelastic scattering $\{A(n,n')A^*\}$, radioactive capture $\{A(n,\gamma)A+1\}$, and other nuclear captures $\{A(n,2n)A-1, A(n,p)A(Z-1), A(n,np)A-1(Z-1), A(n,\alpha), A(n,f)\}$.

Elastic scattering. In an elastic scattering process, kinetic energy and momentum are both conserved. When a neutron scatters elastically from a nucleus, it gives some of its kinetic energy to the nucleus, but the nucleus does not go into an excited state: $X+n \rightarrow X+n$. Since the neutron is small compared with most nuclei, it does not lose much energy in each collision and it can take many collisions to lose its kinetic energy.

Inelastic and capture processes. This covers a number of different mechanisms. In all of them, some of the neutron's kinetic energy is transferred to internal energy of the target nucleus, which is left in an excited state and later decays by emitting neutrons or gamma radiation: $X+n \rightarrow X^*+n$; $X^* \rightarrow X+\gamma$; ${}^{A}_{Z}X^* \rightarrow {}^{A-1}_{Z}Y+n$, etc. For heavy target, nuclei fission may be the preferred break-up mechanism, e.g., ${}_{Z}X+n \rightarrow {}^{Aa}_{Za}X_a+{}^{Ab}_{Zb}X_b$, where $Z = Z_a+Z_b$ and $A = A_a+A_b+1$. The fission fragments X_a and X_b are usually unstable and decay often producing more neutrons. The kind of reaction that occurs depends strongly on the energy of the neutron. The capture reactions occur much more readily for slow neutrons, the attenuation coefficient depending on the velocity as v^{-1}. Thus capture processes are the most important for slow neutrons with kinetic energy less than 0.1 eV. On the other hand, scattering processes are the most important energy loss mechanism for fast neutrons with kinetic energies greater than about 100 keV.

Measurement of ionizing radiation. Standard survey meters are of two types: Geiger counters and ionization chambers. To accurately measure radiation, they must be calibrated by a known

radioactive source, ideally with a wavelength similar to that to be measured. To evaluate a relation between absolute and registered radioactivity, many factors should be taken into account (Lukiyanov et al., 1977): effectiveness of counters to β- and γ-irradiation, weakening of irradiation in the detector walls and in a layer between the substance and the detector, auto-weakening of irradiation, inverse dispersion of irradiation, correction according to the decay scheme of an isotope, geometric conditions of measurements, etc.

Dose units. Dosimetry and biological effects of radiation were recently discussed by Oliveira and Pedroso de Lima (2011). According to the classic data, all organisms are being exposed to ionizing radiation from natural sources all the time. The *roentgen (R)* is a unit of radiation exposure in air. It is defined as the amount of x-ray or gamma radiation that will generate 2.58×10^{-4} C (a measure of electric charge) per kilogram of air at standard temperature and pressure. The absorption of radiation depends on the nature of the absorbing material; thus, the actual energy transferred (i.e., ionization produced in the material) can differ considerably for different materials. Dosages are commonly expressed as R/h (roentgen per hour) or mR/h (milliroentgen per hour). We use two other units to measure this deposited energy. Radiation doses are typically given in units of *rem*—an acronym for *Roentgen equivalent man*—or millirem (mrem), which is one one-thousandth of a rem (a *sievert* is equal to 100 rem). This unit was developed to allow for the consistent reporting of hazards associated with the various types and energies of radiation on the human body. The rem is the product of the absorbed dose in *rads* (i.e., the amount of energy imparted to tissue by the radiation, where 1 rad equals 0.01 J/kg) and factors for the relative biological effectiveness (RBE) of the radiation. The RBE is directly related to the linear energy transfer or distance over which the radiation energy is imparted to the absorbing medium and is accounted for by a quality factor. For example, α-particles are 20 times more hazardous than beta particles for the same energy deposition and hence have a quality factor of 20, whereas the quality factor for β-particles is 1. The International Commission on Radiological Protection has developed a methodology for reporting the effective dose equivalent. This is the product of the dose (in rem or mrem) to individual tissues and the tissue-specific weighting factors (fractional values less than 1) that indicate the relative risk of cancer induction or hereditary defects from irradiation of that tissue, summed over all relevant tissues. By use of the effective dose equivalent, it is possible to compare the relative radiation hazards from various types of radiation that impact different organs of the body.

1.3.5 Recent Studies on the Interaction of Radiation with Matter

Among the important classic contributions in the last years, we note a series of areas of interest, related to distinct elementary particles and dedicated, e.g., to basic *energy transfer* mechanisms and the consequences of ion impact on solids, such as scattering, sputtering, and radiation damage (Fink and Chadderton, 2005). Interaction of *heavy charged particles* with matter (Turner, 2007) and *electromagnetic fields* formed upon the interaction of ionizing radiation with matter (Valiev, 2011) are also intensively studied. Sometimes, unexpected analogies are found. Thus, although the physics describing the interactions of *neutrons with matter* is quite different from that appropriate for hard x-rays and γ-rays, there are a number of similarities that allow analogous instruments to be developed for both types of ionizing radiation (Vanier, 2006). A pinhole camera, e.g., requires that the radiation obeys some form of geometrical optics, that a material can be found to absorb some of the radiation, and that a suitable position-sensitive detector can be built to record the spatial distribution of the incident radiation. Such conditions are met for photons and neutrons, even though the materials used are quite different. Even though the Compton effect applies only to photons, neutrons undergo proton-recoil scattering that can provide similar directional information. *Electron ejection* from target atoms is one of the basic processes when ionizing radiation interacts with matter. The role of the primary ionization (binary encounter and soft electron emission), which is common to single atoms (gas targets) and condensed matter, was discussed (Rothard, 2004), with special emphasis to effects, which are seen only in condensed matter (electron transport and

multiple scattering effects, jet-like structures, wake effects due to collective excitation of plasmons), but not in gaseous targets (single collisions). A teaching module dealing with the *thermal effects* of interaction between radiation and matter, the IR emission of bodies, and the greenhouse effect has been provided (Besson et al., 2010). The module stresses the dependence of the optical properties of materials (transparency, absorptivity, and emissivity) on radiation frequency, as a result of interaction between matter and radiation.

Space ionizing radiation is also an object of permanent studies. It is known that ionizing radiation is an energy source capable of *generating and altering complex organic matter.* The effects of ionizing radiation on a set of 10 naturally occurring, terrestrial organic assemblages (bitumens) were revealed (Court et al., 2006). Progressive radiolytic alteration of biogenic complex–hydrocarbon mixtures induces a decrease in the average size and extent of alkylation of polyaromatic hydrocarbons (PAHs) and an increase in the abundance of oxygen-containing compounds. These changes were attributed to reactions with free radicals, produced by ionizing radiation. Radiolytic alteration is also associated with increase in the mean combustion temperature of organic matter. Results supported proposals that extraterrestrial PAH may be formed by the cosmic irradiation of simple hydrocarbons in interstellar ices. In addition, processes with the use of carbon particles were studied. It is known that in the interstellar medium, dust grains evolve through exposure to UV photons, cosmic rays, gas, heat, and shocks. The results of laboratory studies on the interaction of atomic hydrogen with nanosized carbon particles under simulated interstellar conditions were discussed (Mennella, 2009). This interaction is one of the basic processes for the evolution of the interstellar organic matter during cycling of materials between dense and diffuse regions of the interstellar medium. Other carbon nanomaterials are also objects of intensive investigations. Thus, use of radiation techniques for synthesizing carbon nanomaterials based on fullerenes (Figures 1.10 and 1.11), carbon nanotubes, and graphene sheets and their derivatives, which are promising for practical application due to their unique properties, was reviewed (Gerasimov, 2010). The radiation action of a high-energy electron beam on the carbon surface (soot, graphite, carbon films, etc.) gives rise to different single- and multilayer hollow structures corresponding to fullerenes or onions in shape and size. This process can be represented as the scaling of graphene fragments off the surface of a carbon sample due to the breaking of bonds between carbon atoms and to the formation, by radiation, of defects in the carbon structure followed by the turning of these fragments into small spherical shells, as shown in Figure 1.11. The intensity of the process increases with electron energy in the beam. The threshold energy below which no structural changes are observed in the sample lies in the interval of 40–80 keV.

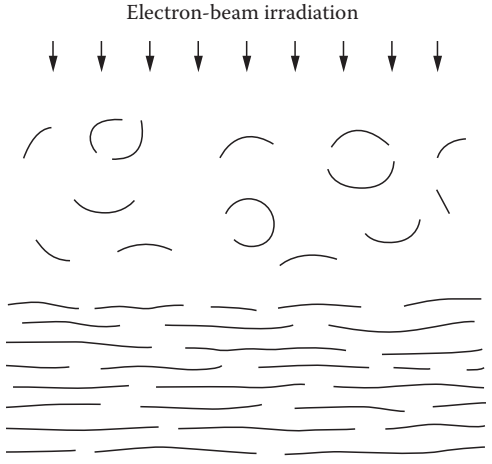

FIGURE 1.10 Formation of fullerene-like shells above the graphite surface under electron-beam irradiation.

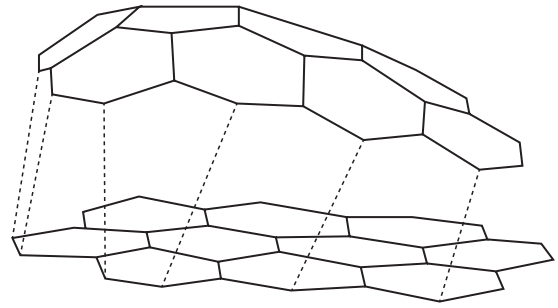

FIGURE 1.11 *Zipper* variant of the coagulation mechanism of formation of fullerenes from two aromatic fragments.

1.4 SYNTHESIS OF MATERIALS APPLYING DISTINCT TYPES OF RADIATION

1.4.1 Irradiation with α-Particles

Alpha particles (helium nuclei $^4_2He^{2+}$) possess classically a total energy of 3–7 MeV. They are a highly ionizing form of particle radiation and have low penetration depth (they are able to be stopped by a few centimeters of air). Currently, their damaging nature is used inside the body by directing small amounts toward a tumor. The alphas damage the tumor and stop its growth while their small penetration depth prevents radiation damage of the surrounding healthy tissue.

There are few examples of their application for synthesis and study of irradiated composites, mainly those of polymers. Sometimes, various irradiation types were used for comparison of produced effects. Thus, the effects of various types of ionizing radiation (γ-rays, electrons, protons, α-particles) on the gas evolution from carbon fiber-reinforced epoxy resin freshly prepared and after storage were studied long ago (Kulikov et al., 1993), resulting that the type of radiation had no effect on the evolution and composition of gases. The composites exhibited high radiation stability. CR-39 and LR-115 plastics were exposed to alpha particles before being irradiated to gamma dose up to the dose of 1.25 MGy (Amin et al., 2000). The plastics were etched and the alpha track diameters were measured after each dose. The diameter of the tracks increased from 3.07 μm with no gamma dose to 85.66 μm when exposed to ~250 kGy for CR-39. In LR-115, the diameter increased from 7.15 μm with no gamma dose to 24.30 μm after dose of ~1.25 MGy. Chemical structure and morphological peculiarities of mesoporous film materials were obtained by the in situ synthesis of cross-linked polycyanurates *via* polycyclotrimerization of dicyanate ester of bisphenol E or A in the presence of linear reactive poly(ε-caprolactone) or poly(tetramethylene glycol), followed by their α-particle irradiation and a track-etching procedure (Fainleib et al., 2009). In comparison with other methods (e.g., using high-boiling phthalate porogens), this technique gave narrower pore size distributions (Grande et al., 2009). An example of inorganic system was reported (Ashurov et al., 1999), describing the analysis of experimental results on photo- and γ-luminescence of zircon crystals, exposed to γ-, α-, and neutron irradiations, as well as annealed natural and synthetic pure $ZrSiO_4$ crystals was performed. An effect of different impurities was examined. A presence of defects was found to be responsible for the yellow luminescence in zircon with a maximum at 580–590 nm.

1.4.2 Irradiation with X-Rays

X-Rays, very common in medicine and in materials characterization, are not so frequently used for production or improvement of properties of materials and composites as the γ-rays or e-beam, described earlier. The products are elemental metals in the form of nanostructures, several oxides, and salts. Thus, reductant, stabilizer-free colloidal gold solutions were fabricated by a new room-temperature *synchrotron x-ray irradiation method* (Yang et al., 2006; Wang et al., 2007).

The characterization included a study of the possible cytotoxicity for the EMT-6 tumor cell line: the negative results indicated that the gold clusters produced with this approach are biocompatible. The polyethylene glycol (PEG)-modified gold nanoparticle complex was prepared by synchrotron x-ray irradiation method (Wang et al., 2008). The size of PEG-modified gold particles was found to decrease with increasing PEG addition and x-ray dosage. The x-ray-prepared PEG–gold nanoparticles could find interesting applications in nanoparticle-enhanced x-ray tumor imaging and therapy. By irradiating a solution in electroless Ni deposition using synchrotron x-rays, Ni composite was found to nucleate homogeneously and eventually precipitate in the form of nanoparticles (100–300 nm) (Lee et al., 2003). By the addition of an organic acid, well-dispersed nanoparticles could be effectively deposited on glass substrate. The authors' results suggested that synchrotron x-ray can be used to induce solution precipitation of nanoparticles and therefore lead to a method of producing nanostructured particles and coating. Ni–Au composite nanoparticles were prepared (Kim and Song, 2006) using synchrotron radiation, exposing a mixed electroless solution of Ni and Au to x-rays at two different temperatures, trying to nucleate Ni nanoparticles homogeneously at room temperature and to deposit Au subsequently on them at the higher temperature of 70°C. The formation of Ni–Au composite nanoparticles was confirmed by the observed ferromagnetic behavior and by the evolution of the Au-surface plasmon resonance band. An electroless deposition method for Ni–P thin films, based on the irradiation by an x-ray beam emitted by a synchrotron source, was described (Hsu et al., 2007). This synthesis is an example of a unique combination of photochemical and electrochemical processes.

Hf-based dielectric films with HfON and HfO_2 gate dielectrics were irradiated by 10 keV x-rays with the dose from 0 to 1×10^6 rad (Si) (Song et al., 2008). Electric measurement results showed that trap charge density and interface trap charge density of HfON dielectric films were much smaller than HfO_2 dielectric films, and the flatband and midgap voltage shifts in HfON films were also smaller than that in HfO_2 film. Additionally, HfON films were smooth and thermally stable even under 800°C high-temperature annealing. In a related investigation, the HfO_2/SiO_2 gel films (the atomic ratio of Si to Hf was about 5:1) were prepared by means of sol–gel technique and exposed to x-ray irradiation (Zhao et al., 2006). After the film was exposed through the mask by x-ray irradiation, a grating, with a highness of 0.8 μm and a period of 1 μm, was fabricated in the HfO_2/SiO_2 sol–gel glass, which showed that the film has a good property of radiation polymerization. Additionally, different thin fluorocarbon (FC) films were deposited on Si(111) using plasma polymerization and then exposed to x-ray radiation (Himmerlich et al., 2008), resulting a high defluorination under x-ray irradiation. With ongoing exposure, the surface charging decreased continuously and the FC surfaces became more conductive due to changes in the polymer structure.

1.4.3 Irradiation with Neutrons

Neutron irradiation, applied mainly for the synthesis of isotopes, e.g., according to $(n;\gamma)$ nuclear reaction, practically is not used for material synthesis or improvement of properties due to possible formation of radioactive isotopes. A few examples are known. Thus, SnO_2 films elaborated by sol–gel method were irradiated (Izerrouken et al., 2009) with reactor neutron at 40°C, with fast neutron fluences ($E_n > 1.2$ MeV) $\leq 9.6 \times 10^{17}$ n/cm^2. It was shown that the resistivity rapidly increased with increasing fluences $\leq 3.2 \times 10^{17}$ n/cm^2 and remained constant for higher fluence ($>6.4 \times 10^{17}$ n/cm^2); the crystallinity and grain size were reduced. Also high-quality sapphire crystal grown by an improved Kyropoulos-like method was irradiated (Wang et al., 2009) by low-energy neutron (i.e., high proportion of thermal neutron) with various flux (low: 7.5×10^{15} n/cm^2, medium: 7.0×10^{16} n/cm^2, and high: 3.8×10^{17} n/cm^2). It was found that sapphire crystal exhibited high radiation resistance to low-energy neutron with low fluence. With the increase in irradiation fluence, it was still sensitive to neutron irradiation mostly in the UV–visible spectral range, as irradiation-induced color centers appear, including F-type and their aggregate centers. Sintered α-SiC ceramics containing B_4C with various ^{10}B concentrations were neutron-irradiated (Pramoto et al., 2003, 2004). The helium release

was observed at various temperatures according to the reaction (1.2). It was supposed that helium will induce some lattice defects into SiC during irradiation, which expanded *c*-axis length of SiC. These defects retained up to 1100°C with support of helium migration, before forming grain boundary bubbles at higher temperature

$$^{10}\mathrm{B} + ^{1}n \rightarrow ^{7}\mathrm{Li}(0.84\ \mathrm{MeV}) + ^{4}\mathrm{He}(1.47\ \mathrm{MeV}) \tag{1.2}$$

$Sc_2@C_{84}$ or Sc_2O_3 was found to be "kicked" into the cavities of single-wall carbon nanotubes (SWNTs) by reactor neutrons (Cao et al., 2007). Experimentally, the open-ended SWNTs were ultrasonically mixed with $Sc_2@C_{84}$ and Sc_2O_3 powders, respectively, in toluene solution, evaporated to dryness, wrapped by high-purity aluminum foils, and then irradiated for 2 h by reactor neutrons. Neutron irradiation also efficiently induced coalescing reactions between two fullerene cages with an atom-spacer, forming a $C_{2m}=C=C_{2n}$ type of carbon nanomaterials (C_{60} powders and $[C_{60}+C_{70}]$ mixture were separately wrapped by high-purity aluminum foils and irradiated for 2 h by neutron beams): C_{141} (formed from two C_{70} molecules), C_{131} (formed from $[C_{60}+C_{70}]$ mixture), and C_{121} (formed from two C_{60} molecules).

1.4.4 Irradiation with Protons

As well as the irradiation with neutrons, the proton irradiation is represented by a few examples, in a difference with heavier ions. Thus, preparation of size- and shape-selective gold nanocrystals (NCs) was achieved through proton beam irradiation from $HAuCl_4$ and $AgNO_3$ solutions (Kim et al., 2010). The shape of the resulting gold NCs was simply controlled by the concentration of the silver ions in the Au growth solution. It was established that Au and Ag ions were co-reduced to form homogeneous Au–Ag composite nanorods under proton beam irradiation. Before introducing radiation damage, the spatial variation of a synthetic single-crystal diamond radiation detector response was investigated (Lohstroh et al., 2008) using a highly focused 2.6 MeV proton beam, showing that a very uniform response close to 100% charge collection efficiency over the whole contact area was found at applied electric field strengths as low as 0.4 V/μm. The darkening of two high OH^- content quartz fibers irradiated with 24 GeV protons was investigated (Cankocak et al., 2007). The fibers became opaque below 380 nm and in the range of 580–650 nm. The darkening under irradiation and damage recovery after irradiation as a function of dose and time are similar to what the authors observed with electrons. The effect of nano-titanium dioxide on mechanical performance of silicone rubber reinforced with MQ resin under the proton radiation with the energy of 100 and 150 keV by space combined radiation system was studied (Di et al., 2006). It was shown that the color of surface of silicon rubber without adding nanoparticle was deepened, the aging crackle was produced on the surface of rubber after irradiation, and the quantity and size of the crackle increased with the increase in irradiation energy and dosage; the hardness and tensile strength increased first and then reduced with the increase in irradiation energy and dosage. Space UV radiation and proton bombardment, which are two of the most important factors that affect the properties of some $BaO–TiO_2$ series microwave dielectric materials in space environment, were simulated in the laboratory (Song et al., 2003), testing dielectric properties of materials. It was shown that the dielectric loss increased after exposing the composite to UV radiation or proton bombardment. However, for $BaTi_4O_9+5$ mol.% Pr samples, the dielectric properties were improved both upon UV irradiation and proton bombardment. MeV proton beams were applied as ionizing radiation to induce graft polymerization of acrylonitrile to prepare amidoxime-type adsorbents on polyethylene film substrates (Kitamura et al., 2004). The degree of grafting (DG) was observed to be proportional to the deposited energy; graft polymerization could be possible deep into a substrate with thickness of hundreds of micrometer, indicating a possibility to control distribution of functional groups with a spatial variation of the order of a micrometer.

1.4.5 Irradiation with Ion Beams

The principles of ion beam synthesis are reviewed elsewhere (Giannuzzi and Stevie, 2004; Kirkby and Webb, 2004; Beyer and von Borany, 2005), in particular its applications for the synthesis and modification of materials (Avasthi, 2009) and nanostructures (Avasthi and Pivin, 2010). A series of charged elemental species (ions of O, C, Si, inert gases, metals, etc.) have been used for ion bombardment of inorganic compounds, polymers, or their composites to obtain advanced materials possessing novel properties. In particular, *metallic beams* are applied very frequently; the low-energy metallic ion beams find wide applications in various research fields of the materials science. Thus, several metallic ion beams have been developed successfully using the *electron cyclotron resonance* ion source-based low-energy ion beam facility (Kumar et al., 2006b). These metallic ion beams, in particular those of Ni (frequently reported) and Fe, were developed by different techniques and utilized for the synthesis of the metal nanoparticles inside various host matrices. Thus, modifications in the structural and optical properties of 100 MeV Ni^{7+}-ion-irradiated cobalt-doped ZnO thin films ($Zn_{1-x}Co_xO$, $x = 0.05$) prepared by sol–gel route were studied (Kumar et al., 2009). The resulted films irradiated with a fluence of 1×10^{13} ions/cm^2 were single phase and show improved crystalline structure with preferred *C*-axis orientation. No change was observed in the bonding structure of ZnO after irradiation. Polymer composites with different concentrations of ferric oxalate dispersed in poly(Me methacrylate) (PMMA) were prepared (Singh et al., 2008) and irradiated with 120 MeV Ni^{10+} ions with fluence of 10^{11}–10^{12} ions/cm^2. It was revealed that the electric conductivity and hardness of the films increased with ferric oxalate concentration and fluence. Commercially available biaxially oriented polypropylene (BOPP) films were irradiated with 90 MeV Ni^{8+} ions and 120 MeV Ag^{11+} ions at different fluencies varying from 10^{10} to 3×10^{11} ions/cm^2 and then grafted with glycidyl methacrylate (GMA) using benzoyl peroxide (BPO) as chemical initiator (Chawla et al., 2009). A comparative study for the GMA grafting using BPO initiator in virgin as well as in the swift heavy ions (SHIs) irradiated BOPP indicated that the heterogeneity of the grafted GMA domains on the BOPP surface was higher in SHI irradiated system. Another example of irradiation with tandem of two different ion beams is obtaining of thin films of CeO_2, prepared on sapphire substrates by sputtering to investigate irradiation-induced degradation of the crystal structure (Ishikawa et al., 2008) of the high-energy heavy ions (200 MeV Au ions and 230 MeV Xe ions from the tandem accelerator). The results revealed that even if ion tracks cover the whole sample, they did not completely destroy the crystal structure, and the lattice order was maintained. The degree of damage in the high-fluence region was higher for 200 MeV Au than for 230 MeV Xe.

Nanocomposite thin films of silver nanoparticles embedded in fullerene C_{60} matrix, prepared by co-deposition of silver and fullerene C_{60} by thermal evaporation, were irradiated (Singhal et al., 2009) by 120 MeV Ag ions at different fluences ranging from 1×10^{12} to 3×10^{13} ions/cm^2. It was revealed that the surface plasmon resonance of Ag nanoparticles showed a blue shift of ~49 nm with increasing ion fluence up to 3×10^{13} ions/cm^2 explained by the transformation of fullerene C_{60} matrix into amorphous carbon. Additionally, growth of Ag nanoparticles was observed with increasing ion fluence. Composite films insulating PMMA, matrix, and Cu powder, prepared by the solution costing method, were irradiated (Singh et al., 2010) with 140 MeV silver ions at the fluences of 1×10^{11} ions/cm^2 and 1×10^{12} ions/cm^2, inducing changes in dielectric, structural, and surface properties of PMMA/Cu composites. It was revealed that ion beam irradiation created free radicals due to emission of hydrogen and/or other volatile gases, which made the polymer more conductive. Al–Sb bilayer thin films having various thicknesses, deposited by thermal evaporation on ITO-coated conducting glass substrates at a pressure of 10^{-5} Torr, were irradiated by Ag^{12+} heavy ions of energy 160 MeV, with a fluence of 2.2×10^{13} ions/cm^2, resulted aluminum antimonide semiconductor (Mangal et al., 2006). It was shown that SHI irradiation process provided approximately same band gap of samples that also indicated different phase formations with thickness due to large diffusion at interface. Gold ions have been also frequently applied (Agarwal et al., 2006); thus, using ion beam cosputtering technique, transparent, light brownish, uniform SiO_2 films embedded with spherical Au

particles were fabricated on quartz substrates at room temperature and heated in an open furnace at different temperature from 500°C to 900°C with 100°C step for 5 min (Gq et al., 2005).

A series of other metal ions have been used for ion beam treatment of composites. Thus, potassium dihydrogen phosphate, which has wide applications as a nonlinear optical material in optoelectronics technology, containing organic dyes (amaranth, rhodamine, and methyl orange), was irradiated (Kumaresan et al., 2007) using 50 MeV Li^+ ions up to a maximum dose of 2.4×10^{15} ions/cm^2. The studies on pure and doped KDP crystals clearly indicated the effect of dopants on the crystal structure. The synthesis of Co nanoparticles by ion implantation was carried out and the effects of postimplantation annealing were discussed (Jacobsohn et al., 2004). Silica was implanted with 35 keV Co^+ ion beams to doses ranging from 8×10^{15} to 1×10^{17} atoms/cm^2. Study of nanoparticle size, distribution, and structure *via* TEM measurements revealed the presence of spherical nanoparticles in both as-implanted and annealed samples. Metallic nanoparticles can be deformed by high-energy ion beams, e.g., metallic cobalt nanoparticles in silica by 200 MeV iodine bombardment (Klaumunzer, 2006). Buried hexagonal AlB_2-type YSi_2 layers were formed by metal vapor vacuum arc implantation of 100 keV Y ions to a dose of 1×10^{18} Y^+ cm^{-2} into *p*-type Si(111) wafers (Wang et al., 2002). It was shown that YSi_2 was formed directly during the implantation, and the implanted region from the surface to the interior of the Si substrate could be divided into four layers based on the concentration profile. The as-implanted sample was metastable, and the stable structure can be formed after irradiation at 530°C. The Group IV NCs were synthesized by 100 keV Ge^+ implantation at 700°C using ion fluences of 1×10^{16} cm^{-2} and subsequent thermal annealing at 1600°C for 120 s (Hedler et al., 2004). Postirradiation was performed by a KrF excimer laser using 1,000–10,000 pulses, laser fluences of 200–500 mJ/cm^2, and pulse durations of 30 ns. It revealed both a reduction of the amount of large NCs and an increase in the amount of small NCs with increasing laser pulses resulting in a reduced mean size and indicating the occurrence of inverse NC ripening processes under laser irradiation.

Various *nonmetallic ions* were found to be able to change properties of materials and composites, in particular silicon ions. Thus, polyaniline thin films prepared by RF plasma polymerization were irradiated with 92 MeV Si ions of fluence of 1×10^{11}, 1×10^{12}, and 1×10^{13} ions/cm^2 (Saravanan et al., 2007). It was shown that the structure of the irradiated sample was altered and the band gap of irradiated thin film was considerably modified. This was attributed to the rearrangement in the ring structure and formation of C≡C terminal groups. The effect of tin impurity and SHI (60 MeV Si^{5+} ion with influence of 5×10^{12} ions/cm^2) irradiation on the optical properties of the chalcogenide thin films was studied (Kumar et al., 2006a). The SHI induced structural and optical changes in the thin films due to which optical band gap decrease. The CdCuS semiconductor nanocrystals were synthesized (Agrawal et al., 2009) by chemical route method, dispersed in PMMA matrix, and then these formed nanocomposite polymer films were irradiated by SHI (100 MeV, Si^{+7} ions beam) at different fluences of 1×10^{10} and 1×10^{12} ions/cm^2. As a result, significant modifications in the structural and optical properties of nanocomposite polymer films were observed. The stability of embedded CdCuS nanocrystals was found to be more than that of its powder form. The surface roughness increased after irradiation. Reduction of the optical band gap may be due to an increase in the defect states near the band tails in the band gap on irradiation. Spherical sub-micrometer-sized silica particles, prepared by the Stoeber process and deposited onto silicon wafers, were then irradiated (Cheang-Wong et al., 2008) at room temperature with Si ions at 8 MeV and fluences up to 5×10^{15} Si/cm^2 (under different angles θ, ranging from 15° to 75° with respect to the sample normal). After the Si irradiation, the as-prepared spherical silica particles turned into ellipsoidal particles, as a result of the increase in the particle dimension perpendicular to the ion beam and a decrease in the direction parallel to the ion beam. This effect increased with the ion fluence. Samples of SiC fiber-reinforced SiC matrix composites were irradiated (Hasegawa et al., 2002) by a simultaneous triple beam of Si^{2+}, He^+, and H^+ at 1000°C and 1300°C. In the SiC composite, no change in the hardness was observed after irradiation at 1000°C, while the hardness of the monolithic β-SiC increased

under these conditions. At 1300°C, the hardness of both SiC fiber composite and monolithic β-SiC decreased after irradiation.

CdS quantum dots were irradiated by 100 MeV C^{+6} SHIs (Gope et al., 2008). Luminescence studies of CaS:Bi nanocrystalline phosphors synthesized by wet chemical co-precipitation method and irradiated with SHIs (i.e., O^{7+}-ion with 100 MeV and Ag^{15+}-ion with 200 MeV) were carried out (Kumar et al., 2007), suggesting a good structural stability of CaS:Bi against SHI irradiation. It was concluded that ion irradiation enhanced the luminescence of the samples. The irradiation of hydroxyapatite (HAp) ceramic was conducted (Parthiban et al., 2008) using oxygen ions at energy of 100 MeV with three different fluences of 10^{12}, 10^{13}, 10^{14} ions/cm^2. It was confirmed an incomplete amorphization of HAp with an increase in fluence; additionally, there was considerable reduction in particle size on irradiation leading to nanosized HAp (up to 53 nm). The irradiated samples exhibited better bioactivity than the pristine HAp. Another example of oxygen ion beam application describes nanostructured polypyrrole films doped with *p*-toluene sulfonic acid, which were prepared by an electrochemical process, and a comparative study of the effects of SHIs and γ-irradiation (oxygen-ion (energy = 100 MeV, charge state = +7) fluence varied from 1×10^{10} to 3×10^{12} ions/cm^2, and the γ-dose varied from 6.8 to 67 Gy) on the structural and optical properties of the polypyrrole was carried out (Chandra et al., 2010). It was shown that after irradiation, the crystallinity improved with increasing fluence because of an increase in the crystalline regions dispersed in an amorphous phase.

As an example *of multiple ion beam irradiations*, we note heavy ion beam-induced epitaxial crystallization of a buried silicon nitride layer (Som et al., 2009). Single crystalline Si(100) samples were first implanted at 300°C with 100 keV N^+ ions to the fluence of 8×10^{17} ions/cm^2 to form the buried nitride layer; the formed samples were further irradiated by 100 MeV O^{8+} ions, 70 MeV Si^{5+}, and 100 MeV Ag^{8+} ions at normal incidence to the constant fluence of 1×10^{14} ions/cm^2 at different temperatures (from room temperature to 250°C). The complete recrystallization of a buried amorphous silicon nitride layer due to Ag and O ions was observed. Oxygen ions led to the recrystallization at 100°C, while the same was achieved at 200°C for the silver ions.

Major part of *inert gases* was also applied. Thus, a polycrystalline zirconolite sample was irradiated (Stennett et al., 2008) with 2 MeV Kr^+ ions at a fluence of 5×10^{15} ions/cm^2. An amorphous character of the irradiated surface was confirmed. To investigate the effect of radiation damage on the stability and the compressive stress of cubic BN (c-BN) thin films, c-BN films with various crystalline qualities, prepared (Zhang et al., 2005) by dual beam ion assisted deposition, were irradiated at room temperature with 300 keV Ar^+ ions over a large fluence $<2 \times 10^{16}$ cm^{-2}. It was shown that the c-BN films with high crystallinity were significantly more resistant against medium-energy bombardment than those of lower crystalline quality. However, even for pure c-BN films without any sp^2-bonded BN, there is a mechanism, which causes the transformation from pure c-BN to h-BN or to an amorphous BN phase. Al nitride films were deposited by varying the voltages of Ar ion beams from 400 to 1200 V in dual ion beam sputtering (Han et al., 2004). The Al nitride films exhibited the <002> preferred orientation at an optimal ion beam voltage of 800 V, changing to a mixture of {100} and {002} planes >800 V, accounting for radiation damage. The thickness of the film increased with increasing ion beam voltage, reaching a steady state value of 210 nm at an ion beam voltage of 1200 V. Poly(ethylene-*co*-tetrafluoroethylene) (ETFE) films were irradiated by SHI beams of $^{129}Xe^{23+}$ with fluences of 0, 3×10^6, 3×10^7, 3×10^8, and 3×10^9 ions/cm^2, followed by γ-ray pre-irradiation for radiation grafting of styrene onto the ETFE films and sulfonation of the grafted ETFE films to prepare highly anisotropic proton-conducting membranes (Kimura et al., 2007). It was found that the polymer electrolyte membrane prepared by grafting the styrene monomer in a mixture of 67% *iso*propanol and 33% water to the ETFE film with an ion beam irradiation fluence of 3.0×10^6 ions/cm^2 was a highly anisotropic proton-conducting material.

Among many other important applications of ion beams, we emphasize their use as a strategic way for the preparation of fuel-cell electrolyte membranes (Kobayashi et al., 2008), involving (a) the irradiation of heavy ions with different masses and energies, (b) the grafting of styrene into

electronically excited region along the ion trajectory called the latent track, and (c) sulfonation of the graft chains. It was established that the property balance of ion-irradiated grafted membrane was found to be better than γ-ray-irradiated grafted membrane. Additionally, 2-D thin films composed of B, C, and nitrogen (B–C–N hybrid), grown (Uddin et al., 2006) from ion beam plasma of borazine on highly oriented pyrolytic graphite at various temperatures, were noted. It was suggested that B, N, and C atoms in the deposited films were in a wide variety of chemical bonds, e.g., B–C, B–N, N–C, and B–C–N. B–C–N hybrid formation was enhanced at high temperature, and the B–C–N component was dominantly synthesized at low B content.

1.5 CONCLUSIONS

Radiation processes in materials, although being a part of classic nuclear physics and chemistry, continue to be objects of permanent research. Together with conventional radiochemical and radiation-chemistry experiments on application of different irradiations for materials synthesis and modifications, some attention is paid to study the influence of cosmic rays on carbon substances, reactions in accelerators and colliders, use of different irradiations at the same time, etc. As a result, various materials and composites can be successfully fabricated or modified by different irradiation techniques with the use of ionizing radiation. The products belong to distinct types of compounds, from inorganic substances (elemental metals, oxides, salts) to a host of polymers, as well as their combinations with the use of oxide or polymer supports. A considerable part of formed composites consists of nanostructures, such as nanoparticles, nanotubes, nanowires, nanofibrils, etc. The obtained products generally possess special properties (e.g., conducting polymers), which can be difficultly or impossibly achieved by conventional methods.

ACKNOWLEDGMENT

The authors are very grateful to Professor *Sergey S. Berdonosov* (Moscow State University, Russia) for critical revision of this manuscript.

REFERENCES

Agarwal, G.; Jain, A.; Agarwal, S.; Kabiraj, D.; Jain, I.P. 2006. Structural and electrical properties of swift heavy ion beam irradiated Co/Si interface. *Bulletin of Material Science*, 29(2):187–191.

Agrawal, S.; Srivastava, S.; Kumar, S.; Sharma, S.S.; Tripathi, B.; Singh, M.; Vijay, Y.K. 2009. Swift heavy ion irradiation effect on Cu-doped CdS nanocrystals embedded in PMMA. *Bulletin of Material Science*, 32(6):569–573.

Amin, Y.M.; Muniandy, S.; Maruthavanam, C. 2000. The effect of gamma radiation on alpha tracks diameter and FTIR spectra of CR-39 and LR-115. *Jurnal Fizik Malaysia*, 21(1–2):51–53.

Ashurov, M.Kh.; Nurildinov, I.; Nazarov, Kh.T.; Vakhidova, M.A. 1999. Luminescence of natural and synthetic zircon crystals. *Doklady Akademii Nauk Respubliki Uzbekistan*, 81(5):13–16.

Avasthi, D.K. 2009. Modification and characterization of materials by swift heavy ions. *Defence Science Journal*, 59(4):401–412.

Avasthi, D.K. and Pivin, J.C. 2010. Ion beam for synthesis and modification of nanostructures. *Current Science*, 98(6):780–792.

Banhart, J. 2008. Radiation sources and interaction of radiation with matter. *Monographs on the Physics and Chemistry of Materials*, 66(Advanced Tomographic Methods in Materials Research and Engineering):107–138.

Bertoni, C.M. 2003. Radiation-matter interaction: Absorption, photoemission, scattering. *Conference Proceedings—Italian Physical Society*, 82(Synchrotron Radiation: Fundamentals, Methodologies and Applications):95–127.

Besson, U.; De Ambrosis, A.; Mascheretti, P. 2010. Studying the physical basis of global warming: Thermal effects of the interaction between radiation and matter and greenhouse effect. *European Journal of Physics*, 31(2):375–388.

Beyer, V. and von Borany, J. 2005. Ion beam synthesis of nanocrystals for multidot memory structures. In: Zschech, E.; Whelan, C.; Mikolajick, T. (Eds.). *Materials for Information Technology*, Part II. Springer, New York, pp. 139–147.

Boon, S.N. 1998. Proton interaction with matter. http://dissertations.ub.rug.nl/FILES/faculties/science/1998/s.n.boon/c2.pdf

Brown, B.A. 1991. Diproton decay of nuclei on the proton drip line. *Physical Review*, C43:R1513–R1517.

Cankocak, K.; Bakirci, N.M.; Cerci, S.; Gulmez, E.; Merlo, J.P.; Onel, Y.; Ozok, F.; Schmidt, I.; Sonmez, N. 2007. Radiation-hardness measurements of high OH-content quartz fibres irradiated with 24 GeV protons up to 1.25 Grad. *CERN Document Server: Preprints*, 1–10:CMS NOTE 2007/003.

Cao, W.; Gao, X.; Qu, L.; Chen, Z.; Xing, G.; Tang, J.; Meng, H.; Chen, Z.; Zhao, Y. 2007. Neutron-irradiation catalyzed synthesis of novel carbon nanomaterials. *Journal of Radioanalytical and Nuclear Chemistry*, 272(3):611–614.

Chandra, S.; Annapoorni, S.; Singh, F.; Sonkawade, R.G.; Rana, J.M.S.; Ramola, R.C. 2010. Effects of an oxygen-ion beam (O^{+7}, 100 MeV) and γ-irradiation on polypyrrole films. *Journal of Applied Polymer Science*, 115(4):2502–2507.

Chawla, S.; Ghosh, A.K.; Avasthi, D.K.; Kulriya, P.K.; Ahmad, S. 2009. Functional polymers synthesized by grafting of glycidyl methacrylate onto swift heavy ions irradiated BOPP films using chemical initiator. *Nuclear Instruments and Methods in Physics Research, Section B*, 267(14):2416–2422.

Cheang-Wong, J.C.; Morales, U.; Resendiz, E.; Lopez-Suarez, A.; Rodriguez-Fernandez, L. 2008. Dependence of the MeV ion-induced deformation of colloidal silica particles on the irradiation angle. *Nuclear Instruments and Methods in Physics Research, Section B*, 266(12–13):3162–3165.

Chmielewski, A.G. 2007. Practical applications of radiation chemistry. *Russian Journal of Physical Chemistry A*, 81(9):1488–1492.

Cole, B.J. 1996. Stability of proton-rich nuclei in the upper *sd* shell and lower *pf* shell. *Physical Review,* C54:1240–1248.

Court, R.W.; Sephton, M.A.; Parnell, J.; Gilmour, I. 2006. The alteration of organic matter in response to ionising irradiation: Chemical trends and implications for extraterrestrial sample analysis. *Geochimica et Cosmochimica Acta*, 70(4):1020–1039.

Di, M.-W.; Zhang, L.-X.; He, S.-Y.; Yang, D.-Z. 2006. Effect of nano-titanium dioxide on mechanical performance of silicone rubber reinforced with MQ resin under proton radiation. *Gaofenzi Cailiao Kexue Yu Gongcheng*, 22(4):122–125.

Drobny, J.G. 2005. Electron beam processing of elastomers. *Rubber World*, 232(4):27–31.

Ehlermann, D.A.E. 2002. Irradiation. In: Henry, C.J.K.; Chapman, C. (Eds.). *Nutrition Handbook for Food Processors*, Woodhead Publishing, Cambridge, U.K., pp. 371–395.

Fainleib, O.M.; Grigor'eva, O.P.; Gusakova, K.G.; Sakhno, V.I.; Zelins'kii, A.G.; Grande, D. 2009. Novel nanoporous thermostable polycyanurates for track membranes. *Fizika i Khimiya Tverdogo Tela*, 10(3):692–696.

Fink, D. and Chadderton, L.T. 2005. Ion-solid interaction: Status and perspectives. *Brazilian Journal of Physics*, 35(3B):735–740.

Gerasimov, G.Ya. 2010. Formation and conversion of carbon nanostructures under radiation. *Journal of Engineering Physics and Thermophysics*, 83(4):849–862.

Giannuzzi, L.A. and Stevie, F.A. (Eds.). 2004. *Introduction to Focused Ion Beams: Instrumentation, Theory, Techniques and Practice*, 1st edn. Springer, New York, 358 pp.

Goldanskii, V.I. 1960. *Nuclear Physics,* 19:482.

Gope, G.; Chakdar, D.; Avasthi, D.K.; Paul, M.; Nath, S.S. 2008. Effect of swift heavy ion on CdS quantum dots embedded in PVA matrix and their applications. In: Laudon, M.; Romanowicz, B. (Eds.). *NSTI Nanotech, Nanotechnology Conference and Trade Show, Technical Proceedings*, June 1–5, 2008, Boston, MA, Vol. 3, pp. 43–45.

Gottschalk, B. 2011.Physics of proton interactions in matter. In: *Proton Therapy Physics*. CRC Press, Boca Raton, FL, Chapter 2, pp. 19–60.

Gq, Y.; Tay, B.K.; Zhao, Z.W.; Sun, X.W.; Fu, Y.Q. 2005. Ion beam co-sputtering deposition of Au/SiO_2 nanocomposites. *Physica E*, 27(3):362–368.

Grande, D.; Gusakova, K.; Grigoryeva, O.; Fainleib, A. 2009. Original approaches to nanoporous cyanurate-based thermosetting films. *PMSE Preprints*, 101:1375–1376.

Han, S.; Chen, H.-Y.; Cheng, C.-H.; Lin, J.-H.; Shih, H.C. 2004. Aluminum nitride films synthesized by dual ion beam sputtering. *Journal of Materials Research*, 19(12):3521–3525.

Hasegawa, A.; Nogami, S.; Igawa, N.; Wakai, E.; Taguchi, T.; Jitsukawa, S. 2002. Effect of multi ion-beams irradiation on mechanical properties of advanced SiC/SiC composites for fusion systems. *JAERI-Review* (2002-035, TIARA Annual Report 2001):136–139.

Hedler, A.; Urban, S.; Kups, T.; Kaiser, U.; Wesch, W. 2004. Laser irradiation of ion beam synthesized Ge nanocrystals in SiC. *Nuclear Instruments and Methods in Physics Research, Section B,* 218:337–342.

Himmerlich, M.; Yanev, V.; Opitz, A.; Keppler, A.; Schaefer, J.A.; Krischok, S. 2008. Effects of X-ray radiation on the surface chemical composition of plasma deposited thin fluorocarbon films. *Polymer Degradation and Stability*, 93(3):700–706.

Hinklin, T. and Lu, K. 2009. *Processing of Nanoparticle Structures and Composites: Ceramic Transactions*, Wiley-American Ceramic Society, New York, Vol. 208, 148 pp.

Hsu, P.-C.; Wang, C.-H.; Yang, T.-Y.; Hwu, Y.-K.; Lin, C.-S.; Chen, C.-H.; Chang, L.-W.; Seol, S.-K.; Je, J.-H.; Margaritondo, G. 2007. Photosynthesis and structure of electroless Ni-P films by synchrotron x-ray irradiation. *Journal of Vacuum Science and Technology A*, 25(3):615–620.

Inokuti, M. 2006. Radiation physics. In: Drake, G.W.F. (Ed.). *Springer Handbook of Atomic, Molecular, and Optical Physics*, Springer, New York, pp. 1389–1399.

Ishikawa, N.; Chimi, Y.; Michikami, O.; Ohta, Y.; Lang, M.; Neumann, R. 2008. X-ray diffraction study of CeO_2 irradiated with high-energy heavy ions. *JAEA-Review* (2007–046):101–102.

Izerrouken, M.; Kermadi, S.; Souami, N.; Sari, A.; Boumaour, M. 2009. Influence of reactor neutrons irradiation on electrical, optical and structural properties of SnO_2 film prepared by sol-gel method. *Nuclear Instruments and Methods in Physics Research, Section A*, 611(1):14–17.

Jacobsohn, L.G.; Hawley, M.E.; Cooke, D.W.; Hundley, M.F.; Thompson, J.D.; Schulze, R.K.; Nastasi, M. 2004. Synthesis of cobalt nanoparticles by ion implantation and effects of postimplantation annealing. *Journal of Applied Physics,* 96:4444–4450.

Kharisov, B.I.; Kharissova, O.V.; Ortiz Mendez, U. 2012. Radiation-assisted synthesis of composites, materials, compounds, and nanostructures. In: Nicolais, L.; Borzacchiello, A.; Lee, S.M. (Eds.). *Wiley Encyclopedia of Composites*, 5 volume set, 2nd edn. Wiley, New York.

Kim, Y.-J. and Song, J.H. 2010. Synthesis of Au-Ag composite nanorods via proton beam irradiation. *Journal of the Korean Physical Society*, 56(6):2072–2076.

Kim, C.-C.; Wang, C.; Yang, Y.-C.; Hwu, Y.-K.; Seol, S.-K.; Kwon, Y.-B.; Chen, C.-H.; Liou, H.-W.; Lin, H.-M.; Margaritondo, G.; Je, J.-H. 2006. X-ray synthesis of nickel-gold composite nanoparticles. *Materials Chemistry and Physics*, 100(2–3):292–295.

Kimura, Y.; Chen, J.; Asano, M.; Maekawa, Y.; Katakai, R.; Yoshida, M. 2007. Anisotropic proton-conducting membranes prepared from swift heavy ion-beam irradiated ETFE films. *Nuclear Instruments and Methods in Physics Research, Section B*, 263(2):463–467.

Kirkby, K.J. and Webb, R.P. 2004. Ion implanted nanostructures. In: Nalwa, H.S. (Ed.). *Encyclopedia of Nanoscience and Nanotechnology*, American Scientific Publishers, Stevenson Ranch, CA, Vol. 4, pp. 283–293.

Kitamura, A.; Hamamoto, S.; Taniike, A.; Ohtani, Y.; Kubota, N.; Furuyama, Y. 2004. Application of proton beams to radiation-induced graft polymerization for making amidoxime-type adsorbents. *Radiation Physics and Chemistry*, 69(2):171–178.

Klaumunzer, S. 2006. Modification of nanostructures by high-energy ion beams. *Nuclear Instruments and Methods in Physics Research, Section B*, 244(1):1–7.

Kobayashi, M.; Yamaki, T.; Nomura, K.; Takagi, S.; Asano, M.; Yoshida, M.; Maekawa, Y. 2008. Development of nanostructure-controlled fuel-cell membranes by ion irradiation technique. Abstracts of Papers, *236th ACS National Meeting*, August 17–21, 2008, Philadelphia, PA, FUEL-108.

Koprda, V. 2005. Radiation chemistry and its application to radiation technology. *NATO Science Series, Series I: Life and Behavioural Sciences*, 365(Radiation Inactivation of Bioterrorism Agents):51–58.

Kulikov, I.A.; Kupriy, A.A.; Nichiporov, F.G.; Yurlova, G.A. 1993. Experimental study on the effect of space factors on durability of carbon fiber-reinforced plastics. 1. Gas evolution from unprotected carbon plastics. *Fizika i Khimiya Obrabotki Materialov*, 1993(1):47–54.

Kumar, V.; Kumar, R.; Lochab, S.P.; Singh, N. 2007. Effect of swift heavy ion irradiation on nanocrystalline CaS:Bi phosphors: Structural, optical and luminescence studies. *Nuclear Instruments and Methods in Physics Research, Section B*, 262(2):194–200.

Kumar, S.; Kumar, R.; Singh, D.P. 2009. Swift heavy ion induced modifications in cobalt doped ZnO thin films: Structural and optical studies. *Applied Surface Science*, 255(18):8014–8018.

Kumar, S.; Laxmi, G.B.V.S.; Husain, M.; Zulfequar, M. 2006a. Effect of SHI irradiation on Se-Te-Sn thin films. *European Physical Journal: Applied Physics*, 35(3):155–158.

Kumar, P.; Rodrigues, G.; Lakshmy, P.S.; Kanjilal, D.; Singh, B.P.; Kumar, R. 2006b. Development of metallic ion beams using ECRIS. *Nuclear Instruments and Methods in Physics Research, Section B*, 252(2):354–360.

Kumaresan, P.; Babu, S.M.; Anbarasan, P.M. 2007. Effect of irradiation of swift heavy ions on dyes doped potassium dihydrogen phosphate crystals for laser applications. *Optoelectronics and Advanced Materials, Rapid Communications*, 1(4):152–157.

L'Annunziata, M.F. 2003. Nuclear radiation, its interaction with matter and radioisotope decay. In: L'Annunziata, M.F. (Ed.). *Handbook of Radioactivity Analysis*, 2nd edn. Oxford Elsevier Ltd., Oxford, U.K., pp. 1–121.

Larson, B. (Ed.). 2012. Interaction of radiation with matter. http://www.ndt-ed.org/EducationResources/CommunityCollege/Radiography/Physics/radmatinteraction.htm

Lee, H.J.; Je, J.H.; Hwu, Y.; Tsai, W.L. 2003. Synchrotron x-ray induced solution precipitation of nanoparticles. *Nuclear Instruments and Methods in Physics Research, Section B*, 199:342–347.

Leroy, C. and Rancoita, P.-G. 2009. *Principles of Radiation Interaction in Matter and Detection*, 2 edn. World Scientific Publishing Company, Singapore, 950 pp.

Lilley, J. 2001. *Nuclear Physics: Principles and Applications*, John Wiley & Sons, New York, pp. 136–142.

Lohstroh, A.; Sellin, P.J.; Gkoumas, S.; Parkin, J.; Veeramani, P.; Prekas, G.; Veale, M.C.; Morse, J. 2008. Ion beam induced charge (IBIC) irradiation damage study in synthetic single crystal diamond using 2.6 MeV protons. *Physica Status Solidi A*, 205(9):2211–2215.

Lukiyanov, V.B.; Berdonosov, S.S.; Bogatyrev, I.O.; Zaborenko, K.B.; Iofa, B.Z. 1977. *Radiotracers in Chemistry. Experiment and Evaluation of Results*, High School, Moscow, Russia, pp. 65–81.

Lukiyanov, V.B.; Berdonosov, S.S.; Bogatyrev, I.O.; Zaborenko, K.B.; Iofa, B.Z. 1985. *Radiotracers in Chemistry. Basis of the Method*, High School, Moscow, Russia, p. 45.

Mangal, R.K.; Singh, M.; Vijay, Y.K.; Avasthi, D.K. 2006. Preparation of Al–Sb semiconductor by swift heavy ion irradiation. *Bulletin of Material Science*, 29(7):653–657.

Mennella, V. 2009. Laboratory studies of the hydrogen-carbon grains interaction: Application to the evolution of the interstellar carbonaceous matter and to molecular hydrogen formation. *Astronomical Society of the Pacific Conference Series*, 414(Cosmic Dust):428–437.

Mozumder, A. and Hatano, Y. 2003. *Charged Particle and Photon Interactions with Matter: Chemical, Physicochemical, and Biological Consequences with Applications*, 1st ed. CRC Press, Boca Raton, FL, 860 pp.

Nave, C.S. 2012. The interaction of radiation with matter. http://hyperphysics.phy-astr.gsu.edu/hbase/mod3.html#c1

Nikjoo, H.; Uehara, S.; Ewfietzoglou, D. (Eds.). 2012. *Radiation Interactions with Matter*, Taylor & Francis Group, Boca Raton, FL, 544 pp.

Oliveira, A.D. and Pedroso de Lima, J.J. 2011. De Lima, J.J.P. (Ed.). Dosimetry and biological effects of radiation. *Nuclear Medicine Physics*, 431–508.

Ormand, W.E. 1996. Properties of proton drip-line nuclei at the sd-fp-shell interface. *Physical Review*, C53:214.

Park, M.V. 2006. Duffus, J.H.; Worth, H.G.J. (Eds.). Radionuclides. *Fundamental Toxicology*, Chapter 21, 273–289.

Parthiban, S.P.; Suganthi, R.V.; Girija, E.K.; Elayaraja, K.; Kulriya, P.K.; Katharria, Y.S.; Singh, F.; Sulania, I.; Tripathi, A.; Asokan, K.; Kanjilal, D.; Yadav, S.; Singh, T.P.; Yokogawa, Y.; Kalkura, S.N. 2008. Effect of swift heavy ion irradiation on hydrothermally synthesized hydroxyapatite ceramics. *Nuclear Instruments and Methods in Physics Research, Section B*, 266(6):911–917.

Piccard, R.D. 2012. Interaction of radiation with matter. http://www.ohio.edu/people/piccard/radnotes/penetrate.html

Poenaru, D.N. and Greiner W. 2011.Cluster radioactivity. In: Beck, C. (Ed.). *Clusters in Nuclei I*, Lecture Notes in Physics 818. Springer, Berlin, Germany, Chapter 1, pp. 1–56.

Pramoto, Y.; Imai, M.; Yano, T. 2003. Helium release and physical property change of neutron-irradiated α-SiC containing B_4C of different ^{10}B concentrations. *Journal of Nuclear Science and Technology*, 40(7):531–536.

Pramono, Y.; Sasaki, K.; Yano, T. 2004. Release and diffusion rate of helium in neutron-irradiated SiC. *Journal of Nuclear Science and Technology*, 41(7):751–755.

Rothard, H. 2004. Track formation and electron emission in swift ion collisions with condensed matter. *Radiotherapy and Oncology*, 73(Suppl. 2):S105–S109.

Saravanan, S.; Anantharaman, M.R.; Venkatachalam, S.; Avasthi, D.K. 2007. Studies on the optical band gap and cluster size of the polyaniline thin films irradiated with swift heavy Si ions. *Vacuum*, 82(1):56–60.

Savchenko, E.V. and Dmitriev, Yu.A. 2010. New aspects of relaxation processes in cryogenic solids. *Horizons in World Physics*, 269(Applied Physics in the 21st Century):113–162.

Schodek, D.L.; Ferreira, P.; Ashby, M.F. 2009. *Nanomaterials, Nanotechnologies and Design: An Introduction for Engineers and Architects*, Butterworth-Heinemann, Oxford, U.K., 560 pp.

Shpak, A.P. and Molodkin, V.V. 2010. Interaction of radiation and particles with condensed matter. Nature of the effect of diffraction conditions on the character of the influence of defects on the dynamic scattering pattern. *Metallofizika i Noveishie Tekhnologii*, 32(11):1435–1467.

Singh, N.L.; Shah, S.; Qureshi, A.; Singh, F.; Avasthi, D.K.; Ganesan, V. 2008. Swift heavy ion induced modification in dielectric and microhardness properties of polymer composites. *Polymer Degradation and Stability*, 93(6):1088–1093.

Singh, D.; Singh, N.L.; Qureshi, A.; Kulriya, P.; Tripathi, A.; Avasthi, D.K.; Gulluoglu, A.N. 2010. Radiation induced modification of dielectric and structural properties of Cu/PMMA polymer composites. *Journal of Non-Crystalline Solids*, 356(18–19):856–863.

Singhal, R.; Agarwal, D.C.; Mishra, Y.K.; Mohapatra, S.; Avasthi, D.K.; Chawla, A.K.; Chandra, R.; Pivin, J.C. 2009. Swift heavy ion induced modifications of optical and microstructural properties of silver-fullerene C_{60} nanocomposite. *Nuclear Instruments and Methods in Physics Research, Section B*, 267(8–9):1349–1352.

Sjirk Niels Boon. 1998. Proton interaction with matter. http://dissertations.ub.rug.nl/FILES/faculties/science/1998/s.n.boon/c2.pdf

Som, T.; Sinha, O.P.; Ghatak, J.; Satpati, B.; Kanjilal, D. 2009. Swift heavy ion beam-induced recrystallisation of buried silicon nitride layer. *Defence Science Journal*, 59(4):351–355.

Song, Z.; Cheng, X.; Zhang, E.; Xing, Y.; Yu, Y.; Zhang, Z.; Wang, X.; Shen, D. 2008. Influence of preparing process on total-dose radiation response of high-k Hf-based gate dielectrics. *Thin Solid Films*, 517(1):465–467.

Song, Y.; Wang, F.; Jiang, Z. 2003. Simulation of the influence of space ultraviolet and proton radiation on dielectric properties of $BaO\text{-}TiO_2$ microwave dielectric ceramics. *Guisuanyan Xuebao*, 31(1):36–40.

Sprawls, P. 2012. Interaction of radiation with matter. http://www.sprawls.org/ppmi2/INTERACT/

Stennett, M.C.; Hyatt, N.C.; Reid, D.P.; Maddrell, E.R.; Peng, N.; Jeynes, C.; Kirkby, K.J.; Woicik, J.C. 2008. Characterization of ion beam irradiated zirconolite for Pu disposition. *Materials Research Society Symposium Proceedings*, Volume Date 2009, 1124 (Scientific Basis for Nuclear Waste Management XXXII): Paper #: 1152-Q10-09.

Tavernier, S. 2010.Interactions of particles in matter. In: *Experimental Techniques in Nuclear and Particle Physics*, Springer, Berlin, Germany, Chapter 2, p. 38.

Trapp, J.V. and Johnston, P. 2008. Fundamentals of radiation physics. In: Trapp, J.V.; Kron, T. (Eds.). *Introduction to Radiation Protection in Medicine*, Taylor & Francis Group, Boca Raton, FL, pp. 19–36.

Turner, J.E. 2004. Interaction of ionizing radiation with matter. *Health Physics*, 86(3):228–252.

Turner, J.E. 2005. Interaction of ionizing radiation with matter. *Health Physics*, 88(6):520–544.

Turner, J.E. 2007. Interaction of heavy charged particles with matter. In: *Atoms, Radiation, and Radiation Protection*, 3rd edn. Wiley, Berlin, Germany, Chapter 5.

Uddin, Md.N.; Shimoyama, I.; Sekiguchi, T.; Nath, K.G.; Baba, Y.; Nagano, M. 2006. Preparation and characterization of B-C-N hybrid thin films. *JAEA-Research* (2006–034), i–xii:1–72.

Valiev, F.F. 2011. Electromagnetic fields formed upon the interaction of ionizing radiation with matter. *Bulletin of the Russian Academy of Sciences: Physics*, 75(7):1001–1006.

Vanier, P.E. 2006. Analogies between neutron imaging and gamma-ray imaging. *Proceedings of SPIE-The International Society for Optical Engineering*, 6319(Hard X-Ray and Gamma X-Ray Detector Physics and Penetrating Radiation Systems VIII):63190E/1-63190E/8.

Wang, G.-G.; Han, J.-C.; Zhang, H.-Y.; Zhang, M.-F.; Zuo, H.-B.; Hu, Z.-H.; He, X.-D. 2009. Radiation resistance of synthetic sapphire crystal irradiated by low-energy neutron flux. *Crystal Research and Technology*, 44(9):995–1000.

Wang, C.H.; Hua, T.E.; Chien, C.C. et al. 2007. Aqueous gold nanosols stabilized by electrostatic protection generated by X-ray irradiation assisted radical reduction. *Materials Chemistry and Physics*, 106(2):323–329.

Wang, C.-H.; Liu, C.-J.N.; Wang, C.-L.; Hua, T.-E.; Obliosca, J.M.; Lee, K.H.; Hwu, Y.; Yang, C.-S.; Liu, R.-S.; Lin, H.-M.; Je, J.-H.; Margaritondo, G. 2008. Optimizing the size and surface properties of polyethylene glycol (PEG)-gold nanoparticles by intense X-ray irradiation. *Journal of Physics D*, 41(19):195301/1–195301/8.

Wang, W.; Xie, E.; Jiang, N.; He, D. 2002. Ion beam synthesis and characterization of yttrium silicide. *Applied Surface Science*, 199(1–4):1–5.

Yang, Y.C.; Wang, C.H.; Hwu, Y.K.; Je, J.H. 2006. Synchrotron X-ray synthesis of colloidal gold particles for drug delivery. *Materials Chemistry and Physics*, 100(1):72–76.

Yi, X.-S.; Du, S.; Zhang, L. 2010. *Composite Materials Engineering*, 1st edn. Springer, Berlin, Germany, Vol. 29, 2900 pp.

Zaborenko, K.B.; Iofa, B.Z.; Lukiyanov, V.B.; Bogatyrev, I.O. 1964. *Method of Radiotracers in Chemistry*, High School, Moscow, Russia, pp. 37–38.

Zhang, X.W.; Yin, H.; Boyen, H.-G.; Ziemann, P.; Ozawa, M. 2005. Effects of crystalline quality on the phase stability of cubic boron nitride thin films under medium-energy ion irradiation. *Diamond and Related Materials*, 14(9):1482–1488.

Zhao, F.-H.; Xie, Y.-J.; Xu, S.-L.; Liu, G.; Fu, S.-J. 2006. Preparation of HfO_2-SiO_2 sol-gel glass with radiation polymerization properties and studies of its X-ray lithography properties. *Gaodeng Xuexiao Huaxue Xuebao*, 27(7):1376–1379.